Received: 13 January 2022 | Revised: 3 April 2022 | Accepted: 14 May 2022

DOI: 10.1002/rnc.6218

RESEARCH ARTICLE

WILEY

Adaptive robust path tracking control for autonomous vehicles with measurement noise

Huiqian Li[1] | **Jin Huang**[1] | **Zeyu Yang**[2] | **Zhanyi Hu**[1] | **Diange Yang**[1] | **Zhihua Zhong**[1,3]

[1]School of Vehicle and Mobility, Tsinghua University, Beijing, China

[2]College of Mechanical and Vehicle Engineering, Hunan University, Changsha, Hunan, China

[3]Chinese Academy of Engineering, Beijing, China

Correspondence
Jin Huang, School of Vehicle and Mobility, Tsinghua University, Beijing 100084, China.
Email: huangjin@tsinghua.edu.cn

Funding information
Ministry of Science and Technology of the People's Republic of China, Grant/Award Number: 2020YFB1710901; National Natural Science Foundation of China, Grant/Award Numbers: 61872217, U20A20285, 52122217, U1801263

Abstract

In practical autonomous vehicle systems, model uncertainty and measurement noise are two challenging factors that deteriorate path tracking accuracy and system stability. This article proposes an adaptive robust controller to deal with these two factors and enhance path tracking accuracy. First, the path tracking model considering time-varying uncertainty is built and represented as nominal and uncertain portions. Second, the control law is designed separately for both portions. A linear quadratic regulator controller is utilized to stabilize the nominal system. An additional robust control law is proposed to suppress the matched uncertainty and measurement noise, with an adaptive scheme aimed at estimating the bound outside uncertainty. The path tracking system with the developed control law is proved to possess uniform boundedness, uniform ultimate boundedness properties, and robustness against mismatched uncertainty. Eventually, the effectiveness of the developed controller is validated using both MATLAB/Simulink-TruckSim co-simulation and an autonomous vehicle platform. The results demonstrate that the designed adaptive robust control can achieve accurate path tracking in the presence of time-varying uncertainty and measurement noise.

KEYWORDS

adaptive control, autonomous vehicle, measurement noise, path tracking, robust control

1 | INTRODUCTION

Autonomous vehicles (AVs) have the capability to navigate themselves depending on surrounding environments and scheduled tasks. Typical autonomous vehicle systems consist of three basic stages and modules, namely perception, planning, and control.[1] Control strategies play a significant role in finishing the expected driving tasks. The control strategy is usually decoupled into longitudinal and lateral control. This article focuses on path tracking control, which enables a vehicle to track its desired path.

The path tracking problem has been widely studied recently.[2-6] Existing path tracking strategies can be categorized into two types, that is, model-free methods and model-based methods. Model-free methods have the advantages of simplicity and ease of engineering application, such as PID control and fuzzy control methods.[7] In recent years, some learning-based methods have also gained increasing popularity.[8,9] As for model-based strategies, the vehicle model and controller design

are two significant points to improve the performance of path tracking for autonomous vehicles. The frequently used model configurations include geometric, kinematic, and dynamic models.[10] Each of them has its benefits and purposes depending on usage and studied properties. The pure pursuit algorithm and Stanley method are two popular geometric controllers and can achieve satisfactory performance at a relatively low speed.[11,12] Methods based on optimization theories, such as linear quadratic regulator (LQR) and model predictive control (MPC), have been widely used to design path tracking controllers.[13,14] They have the potential to enhance path tracking accuracy at the cost of increased computational burden. In practical vehicle systems, model uncertainty and measurement noise are two challenging factors that influence path tracking performance, whereas the aforementioned methods do not address them explicitly. To further improve the path tracking accuracy, robustness against these two factors should be considered in designing path tracking controllers.

Time-varying uncertainty is unavoidable for model-based path tracking control strategies, due to the simplifications and idealizations made in model formulations. The existence of time-varying uncertainty may result in poor tracking performance or even unsteady motions, which can be dangerous for autonomous vehicles. Extensive efforts have been dedicated to robust path following controllers design.[15-18] Chen et al.[19] investigated the robust $H\infty$ path tracking control design of network-based autonomous vehicles with delay and packet dropout. Tagne et al.[20] proposed a higher-order sliding-mode controller, and verified the robustness against the incorrect value of tire stiffness coefficient and vehicle mass. The robust MPC theory has also been proposed and adopted for the path tracking task in recent years.[21,22] This method introduced the characteristics of parametric uncertainties, external disturbance, time-varying, and non-linearities into the autonomous vehicle model, and dealt with the inevitable model mismatch problem caused by them. Experimental results verified that this strategy could strengthen the robustness of the controlled system and achieve better path tracking accuracy.[21] Yang et al.[18] innovatively formulated the vehicle path tracking task as a constraint-following problem and proposed an optimal robust control for autonomous vehicles with fuzzy uncertainties. Nevertheless, these control strategies are usually based on a precisely known bound, which is not suitable for practical engineering systems without the knowledge of uncertainty bounds.

Apart from model uncertainty, measurement noise of system state is also inevitable in engineering systems. The noise resulting from sensors has an impact on the smoothness and stability of the path tracking system. Valuable explorations have been done to handle measurement noise in the process of controller design.[23-26] Most of the existing studies focus on filtering the noise out. Lee et al.[23] designed a model-based linear quadratic Gaussian (LQG) control with an adaptive Q-matrix and validated its performance by experimental results. The controller could effectively handle the noise and errors arising from the localization and path planning algorithm. Rayguru et al.[26] developed a robust observer-based sliding mode controller to fulfill the path tracking task under sensor inaccuracies. The designed controller performed well under measurement errors but it could barely account for any model uncertainties. Although the measurement noise can be reduced by various filter algorithms, it can not be eliminated. Thus, in the process of controller design, it is necessary to assure closed-loop stability in the presence of measurement noise.

To improve the path tracking performance of autonomous vehicles, the controller needs to be robust against both model uncertainties and measurement noise. In this article, the designed controller consists of two parts, one of which aims to stabilize the nominal system, namely the system without considering model uncertainties, and the other is used to counteract the impact of model uncertainties and measurement noise.

Hence, based on the LQR controller, we develop an adaptive control law to suppress the matched uncertainties. Furthermore, we discuss its robustness against mismatched uncertainties and measurement noise. Finally, the proposed controller is implemented on both the simulation platform and vehicle platform to validate its effectiveness.

The main contribution of this article is the design and validation of the adaptive robust path tracking controller that can tackle both model uncertainty and measurement noise. Specifically, the study contributes in two ways: (a) A robust path tracking controller is designed to compensate for model uncertainty and measurement noise, with an adaptive law to approximate their bounds. The proposed controller renders the uniform boundedness (UB) and the uniform ultimate boundedness (UUB) performance of the path tracking system. The performance is guaranteed in theory and validated through both simulation and field tests. (b) The robustness of the proposed controller against mismatched uncertainties is analyzed, and the sufficient condition ensuring the robustness is provided.

The remainder of this article is outlined as follows. Section 2 derives the vehicle lateral dynamics model and path tracking problem formulation. Section 3 introduces the design of the controller. Section 4 analyzes the performance of the proposed controller and its robustness against the mismatched uncertainties. The simulation and experimental results are described and discussed in Section 5. Section 6 concludes the article.

2 | MODELING OF PATH TRACKING SYSTEM

In this section, a path tracking model based on the vehicle lateral dynamic model is built. Then the uncertainties contained in the model are analyzed, and divided into matched and mismatched portions.

2.1 | Vehicle lateral dynamic model

This article focuses on controller design for front-wheel-steering vehicles. We suppose that the vehicle body and the suspension system are rigid, and the vertical motion can be ignored. The steering motion is driven by the front steer only, and we assume that the tires have the same steering angle and speed at any moment. A linear single-track dynamic model considering lateral motion and yaw motion is adopted to design the path tracking controller. This dynamic model keeps the essential vehicle steering dynamics, as well as low computational complexity. The definitions of the inertial coordinate system *OXY* and the vehicle local coordinate system *oxy* are depicted in Figure 1. Corresponding symbols are explained in Table 1.

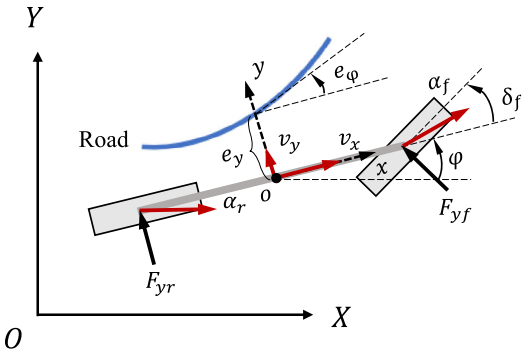

FIGURE 1 Coordinate system layout of the path tracking problem.

TABLE 1 Definitions and symbols of the dynamics model

Definition	Symbol	Unit
Mass of the vehicle	m	kg
Longitudinal velocity (in *oxy*)	v_x	m/s
Lateral velocity (in *oxy*)	v_y	m/s
Lateral acceleration (in *oxy*)	a_y	m/s^2
Heading angle of vehicle body (in *OXY*)	φ	rad
Yawing moment of inertia of the vehicle	I_z	kg m^2
Front wheel steering angle	δ_f	rad
Lateral tire force of the front/rear wheel (in *oxy*)	F_x, F_y	N
Distance from c.g. to the front/rear axle	l_f, l_r	m
Slip angle of the front/rear wheel	α_f, α_r	rad
Cornering stiffness of vehicle of the front/rear axle	C_f, C_r	N/rad
Road curvature	c_R	1/m
Heading error of vehicle with respect to road	e_φ	rad
Offset of c.g. from the trajectory	e_y	m
Desired heading of vehicle body (in *OXY*)	φ_{des}	rad

According to Newton's second law, the dynamic equations of the lateral and yaw motions can be written as

$$\begin{aligned} m(\dot{v}_y + v_x\dot{\varphi}) &= F_{yf} + F_{yr}, \\ I_z\ddot{\varphi} &= l_f F_{yf} - l_r F_{yr}, \end{aligned} \tag{1}$$

where F_{yf} and F_{yr} are the lateral tire forces of the front and rear tires, respectively. Under the small slip-angle assumption, they are proportional to the tire slip angles, namely

$$F_{yf} = C_f\alpha_f, F_{yr} = C_r\alpha_r, \tag{2}$$

where C_f and C_r are cornering stiffness of the front and rear axles; α_f and α_r are slip angles of the front and rear wheels.

The slip angles in Equation (2) can be obtained by

$$\alpha_f = -\frac{v_f}{v_x} + \delta_f = -\frac{v_y + l_f\dot{\varphi}}{v_x} + \delta_f, \quad \alpha_r = -\frac{v_r}{v_x} = -\frac{v_y - l_r\dot{\varphi}}{v_x}, \tag{3}$$

where v_f and v_r are the lateral speeds of the front and rear wheel, respectively.

Figure 1 describes the definitions of the errors in the path tracking problem. The lateral error e_y stands for the distance between the gravity center and the reference waypoint that is defined by the crosspoint of the reference path and the y axis. Similarly, the heading error e_φ is calculated by the desired heading angle of the reference waypoint minus the current heading angle. The above definitions indicate that the studied tracking problem is a geometric path-following problem.[27] Combining Equations (1)–(3), we can express the second order derivative of lateral error e_y and heading error e_φ as

$$\begin{aligned} \ddot{e}_y &= \frac{C_f}{m}\delta_f - \frac{C_f + C_r}{mv_x}(\dot{e}_y - v_x e_\varphi) - \left[\frac{l_f C_f - l_r C_r}{mv_x}\right](\dot{e}_\varphi + \dot{\varphi}_{\text{des}}) + v_x\dot{e}_\varphi, \\ \ddot{e}_\varphi &= \frac{l_f C_f}{I_z}\delta_f - \frac{l_f C_f - l_r C_r}{I_z v_x}(\dot{e}_y - v_x e_\varphi) - \frac{l_f^2 C_f + l_r^2 C_r}{I_z v_x}(\dot{e}_\varphi + \dot{\varphi}_{\text{des}}) - \ddot{\varphi}_{\text{des}}. \end{aligned} \tag{4}$$

The lateral dynamics can be denoted in the state-space form, with the state vector being $x = [e_y, \dot{e}_y, e_\varphi, \dot{e}_\varphi]^{\mathrm{T}} \in \mathbb{R}^4$ and the control input being the front wheel steering angle $u = \delta_f \in \mathbb{R}$, that is,

$$\dot{x} = \begin{bmatrix} 0 & 1 & 0 & 0 \\ 0 & \frac{\hat{a}_1}{mv_x} & \frac{\hat{a}_1}{m} & \frac{-\hat{a}_2}{mv_x} \\ 0 & 0 & 0 & 1 \\ 0 & \frac{-\hat{a}_2}{I_z v_x} & \frac{\hat{a}_2}{I_z} & \frac{-\hat{a}_3}{I_z v_x} \end{bmatrix} x + \begin{bmatrix} 0 \\ \frac{C_f}{m} \\ 0 \\ \frac{l_f C_f}{I_z} \end{bmatrix} u + \begin{bmatrix} 0 \\ \frac{-\hat{a}_2}{m} - v_x^2 \\ 0 \\ \frac{-\hat{a}_3}{I_z} \end{bmatrix} c_R, \tag{5}$$

where $\hat{a}_i (i = 1, 2, 3)$ are the lumped coefficients defined as

$$\hat{a}_1 = C_f + C_r, \quad \hat{a}_2 = l_f C_f - l_r C_r, \quad \hat{a}_3 = l_f^2 C_f + l_r^2 C_r. \tag{6}$$

Then the state-space equation of the path tracking problem can be simplified as

$$\dot{x} = \hat{A}x + \hat{B}u + Dc_R. \tag{7}$$

The output equation can be written as

$$y = x + w, \tag{8}$$

where $w \in \mathbb{R}^4$ denotes the measurement noise.

2.2 | Uncertainty analysis

In real-world engineering systems, the model uncertainty may arise from various sources, such as parametric perturbation and unmodeled disturbance. Many ways to describe uncertainty have been applied in existing studies. In References 28,29, probability theory was employed to interpret the uncertainties. This approach describes the distribution of the uncertainties, but sufficient data is needed to calculate the frequency of occurrence. Xu et al.[30] and Yang et al.[18] model the uncertainties using fuzzy set theory, which adopts the degree of occurrence to describe uncertainty. Besides, uncertainty bound is another frequently used method to describe uncertainty, which complies with the fact that engineering system uncertainties usually have bounds.[31] Here we mainly analyze the parametric uncertainty of the path tracking dynamic model, by decomposing the parameters with uncertainty.

In real-world vehicle systems, it is hard to acquire the tire cornering stiffness exactly due to its nonlinearity. Consider the parametric uncertainty of the cornering stiffnesses C_f and C_r, that is,

$$C_f = \overline{C}_f + \Delta C_f, C_r = \overline{C}_r + \Delta C_r, \tag{9}$$

where $\overline{C}_f$ and $\overline{C}_r$ denote the nominal portion, that is, a deterministic value set in the model; ΔC_f and ΔC_r represent the uncertain portion, that is, the discrepancy between the value of the nominal portion and the true value.

Hence, the path tracking dynamic model can be rewritten in terms of nominal portions and uncertain portions as

$$\begin{aligned} \dot{x} &= \hat{A}x + \hat{B}u + Dc_R \\ &= (A + \Delta A)x + (B + \Delta B)u + Dc_R \\ &= (Ax + Bu) + (\Delta Bu + \Delta Ax + Dc_R), \end{aligned} \tag{10}$$

where the matrices A, ΔA, B, and ΔB can be calculated using Equations (5) and (9).

We decompose the uncertain coefficient matrices along the direction of nominal input matrix B. For ΔA, we have

$$\Delta A = BA_1 + A_2, \tag{11}$$

where

$$A_1 = \begin{bmatrix} 0 & \frac{-\Delta C_f}{\overline{C}_f v_x} & \frac{\Delta C_f}{\overline{C}_f} & \frac{-l_f \Delta C_f}{\overline{C}_f v_x} \end{bmatrix}, A_2 = \begin{bmatrix} 0 & 0 & 0 & 0 \\ 0 & \frac{-\Delta C_r}{m v_x} & \frac{\Delta C_r}{m} & \frac{l_r \Delta C_r}{m v_x} \\ 0 & 0 & 0 & 0 \\ 0 & \frac{l_r \Delta C_r}{I_z v_x} & \frac{-l_r \Delta C_r}{I_z} & \frac{-l_r^2 \Delta C_r}{I_z v_x} \end{bmatrix}. \tag{12}$$

As for ΔB, it can be denoted as

$$\Delta B = Bb, \tag{13}$$

where $b = \frac{\Delta C_f}{\overline{C}_f}$.

Similarly, matrix D can be decomposed as

$$D = Bd + D_1, \tag{14}$$

where

$$d = -\frac{C_f l_f}{\overline{C}_f} - \frac{m l_r}{\overline{C}_f (l_f + l_r)} v_x^2, \quad D_1 = \begin{bmatrix} 0 \\ \frac{l_r C_r}{m} - \frac{l_f}{l_f + l_r} v_x^2 \\ 0 \\ \frac{-l_r^2 C_r}{I_z} + \frac{m l_f l_r}{I_z (l_f + l_r)} v_x^2 \end{bmatrix}. \tag{15}$$

Substituting Equations (11), (13), and (14) into state-space equation (10), we have

$$\begin{aligned}\dot{x} &= Ax + Bu + (\Delta Bu + \Delta Ax + Dc_R)\\ &= Ax + B(1+b)u + B(A_1x + dc_R) + (A_2x + D_1c_R)\\ &:= Ax + B(1+b)u + e + \tilde{e},\end{aligned} \tag{16}$$

where

$$e = B(A_1x + dc_R), \quad \tilde{e} = A_2x + D_1c_R. \tag{17}$$

So far, the path tracking dynamical model has been rewritten as the formulation with the matched uncertainty e and the mismatched uncertainty $\tilde{e}$. The matched uncertainty enters the system through the same channel as the control input, while the mismatched part enters the system in an arbitrary manner. Thus, we can restrain the matched portion of the uncertainty by assigning a certain control force. On the other hand, the mismatched uncertainty existing in the path tracking system can be tolerated in order to ensure system stability. Next, we will begin with designing a controller based on the model considering only matched uncertainty. The capability of tolerating mismatched uncertainty will be discussed later.

3 | ADAPTIVE ROBUST PATH TRACKING CONTROL DESIGN

We design the controller with two targets, stabilizing the nominal system and compensating for the uncertain part and measurement noises. In this section, we design a control law related to these two targets.

Consider the following path tracking system with uncertainties and measurement noises

$$\begin{cases}\dot{x}(t) = Ax(t) + Bu(t) + e(x,\sigma,t),\\ y(t) = x(t) + w(t),\end{cases} \tag{18}$$

where $e(x,\sigma,t)$ denotes the uncertain portion of the system, and $\sigma \in \Sigma \subset \mathbb{R}^m$ represents the uncertainty parameter of the path tracking dynamical system. $w \in W \subset \mathbb{R}^4$ represents the uncertainty parameter of the measurement noise. Σ and W are unknown but compact. As σ is only contained by the uncertain portions of the parameters, we use $e(x,t)$ in the following context for simplicity. However, the mismatched uncertainty $\tilde{e}$ is neglected. In the following context, we will show that this simplification does not hurt its robustness against mismatched uncertainties.

For uncertain system Equation (18), the following control is designed

$$u(t) = Ky(t) + p(y(t), \hat{\beta}(t)), \tag{19}$$

where $u_1 = Ky(t)$ is designed to stabilize the nominal portion and $u_2 = p(y(t), \hat{\beta}(t))$ aims to compensate for uncertain portion with adaptive parameter $\hat{\beta}(t)$.

First, to stabilize the nominal system, we consider the Riccati equation

$$A^{\mathrm{T}}P + PA - 2PBR^{-1}B^{\mathrm{T}}P + Q = 0, \tag{20}$$

where $Q \in \mathbb{R}^{4\times4}$ is a constant positive semi-definite matrix and $R \in \mathbb{R}$ is a positive constant scalar. The solution of the equation has a unique existence because the pair (A,B) is stabilizable. Hence, the feedback coefficient can be given by

$$K = -R^{-1}B^{\mathrm{T}}P. \tag{21}$$

Next, the second portion of u is designed to suppress the uncertainty. The saturation type control $p(y,\hat{\beta})$ is given by

$$p(y,\hat{\beta}) = \begin{cases} -\frac{B^{\mathrm{T}}Py}{\|B^{\mathrm{T}}Py\|}(\hat{\beta}_1 + \hat{\beta}_2\|y\|) & \text{if } \|B^{\mathrm{T}}Py\| > \epsilon\\ -\frac{B^{\mathrm{T}}Py}{\epsilon}(\hat{\beta}_1 + \hat{\beta}_2\|y\|) & \text{otherwise}\end{cases}, \tag{22}$$

where ϵ is a small positive constant in case the denominator is equal to zero. The parameter $\beta = [\beta_1, \beta_2]^{\mathrm{T}}$ of the bounds of uncertainties, represented as $\beta_1 + \beta_2\|y\|$, is unknown. Hence, $\hat{\beta}_1$ and $\hat{\beta}_2$ are used to approximate them in the following adaptive scheme.

Throughout this article, vector norms $\|\cdot\|$ are taken to be 2-norm if no specific subscripts are marked, and the matrix norms are the corresponding induced ones. That is, $\|\mathbf{\Sigma}\|^2 = \lambda_M(\Sigma^{\mathrm{T}}\Sigma)$, where Σ is a real matrix, $\lambda_M(\cdot)$ and $\lambda_m(\cdot)$ represent the maximum and minimum eigenvalues of the matrix.

Then the adaptive scheme for $\hat{\beta} = [\hat{\beta}_1, \hat{\beta}_2]$ is given as

$$\dot{\hat{\beta}}(t) = \begin{cases} L_1 g(y)\|B^{\mathrm{T}}Py\| - L_2\hat{\beta}(t) - L_3\hat{\beta}(t)\|y\| & \text{if } \|B^{\mathrm{T}}Py\| > \epsilon \\ L_1 g(y)\frac{\|B^{\mathrm{T}}Py\|^2}{\epsilon} - L_2\hat{\beta}(t) - L_3\hat{\beta}(t)\|y\| & \text{otherwise} \end{cases}, \tag{23}$$

where L_1, L_2, and L_3 are given positive definite 2×2 matrices, and $g(y) = [1, \|y\|]^{\mathrm{T}}$. The initial value of $\hat{\beta}$ is denoted as $\hat{\beta}(t_0) = \hat{\beta}_0$.

The motivation for this adaptive scheme stems from the following. First, as the system performance deteriorates, a mechanism should be provided so that the scheme can become more dominant. Second, the scheme should be capable of adaptively adjusting its strategy when the system performance is satisfied. In adaptive scheme Equation (23), the first term grows rapidly with $\|B^{\mathrm{T}}Py\|$ increasing, which indicates that the system performance worsens. The second and third terms determine the decreasing rate. If $\|y\|$ is small or $\hat{\beta}$ is large, the decreasing rate becomes significant.

Lemma 1. *(i) For given path tracking system Equation (18) and control law Equation (19) with adaptive scheme Equation (23), there exists a function $\hat{e}$, such that for all x*

$$e(x,t) = B\hat{e}(x,t). \tag{24}$$

(ii) Further, there are constants $k_1 \geq 0$ and $k_2 \geq 0$ so that for all x, we have

$$\|e(x,t)\| \leq k_1 + k_2\|x\|. \tag{25}$$

Here Equation(25) means that $\hat{e}$ is cone-bounded *but the bounds k_1 and k_2 are unknown.*

Proof of Lemma 1. (i) According to Equation (16) and control law Equation (19), ignoring the mismatched uncertainty term, we have

$$e(x,t) = B[Kw + A_1x + b(Kx + Kw + p(x + w, \hat{\beta})) + dc_R], \tag{26}$$

so for all x, we have

$$\hat{e}(x,t) = Kw + A_1x + b(Kx + Kw + p(x + w, \hat{\beta})) + dc_R. \tag{27}$$

(ii) Then we first assume that $\hat{e}(x,t)$ is cone-bounded. That is, there exist unknown positive parameters θ_1 and θ_2 making the following equation solvable

$$\|\hat{e}(x,t)\| \leq \theta_1 + \theta_2\|x\|. \tag{28}$$

For $y = x + w$,

$$\begin{aligned} \|\hat{e}(x,t)\| &\leq \|Kw\| + \|A_1\|\|x\| + \|bK\|\|x + w\| + \|b\|(\hat{\beta}_1 + \hat{\beta}_2\|x + w\|) + \|dc_R\| \\ &\leq \max_{w\in W}\|Kw\| + \max_{\sigma\in\Sigma}(\|A_1\| + \|bK\| + \|b\|\hat{\beta}_2)\|x\| + \max_{w\in W,\sigma\in\Sigma}(\|bKw\| + \hat{\beta}_2\|bw\|) + \max_{\sigma\in\Sigma}(\hat{\beta}_1\|b\| + \|dc_R\|), \end{aligned} \tag{29}$$

where $\sigma \in \Sigma \subset \mathbb{R}^m$ and $w \in W \subset \mathbb{R}^4$ represent the uncertainty parameters of the system and the measurement noise, respectively. Σ and W are unknown but compact. Additionally, according to the adaptive law Equation (23), letting $\dot{\hat{\beta}} = 0$, the adaptive parameters achieve the maximum value

$$\max_{t\in\mathbb{R}}\hat{\beta}(t) = L_1 g(y)\|B^T Py(\|L_2 + L_3\|y\|)^{-1}. \tag{30}$$

Near the equilibrium state, $\|y\|$ is bounded, so the adaptive parameters are bounded. Since in the real-world dynamical system both system uncertainty and measurement noise are bounded too, there exist positive constants θ_1 and θ_2 that make the assumption Equation (28) reasonable.

Combine Equations (24) and (28)

$$\|e(x,t)\| \le \|B\|\|\hat{e}(x,t)\| \le \|B\|(\theta_1 + \theta_2\|x\|) = k_1 + k_2\|x\|. \tag{31}$$

Hence, Lemma 1 is proved. ∎

Definition 1. *Uniform boundedness.* Given any $r > 0$ and any $\mu(\cdot) : [t_0, t_1) \to \mathbb{R}^4 \times \mathbb{R}^2$, $\mu(t_0) = \mu_0$, of the closed-loop system, with $\|\mu_0\| \le r$, there is a constant $d(r) > 0$ such that $\|\mu(t)\| \le d(r)$ for all $t \in [t_0, t_1)$.

Definition 2. *Uniform ultimate boundedness.* For each $\bar{d} \ge d$ and $r > 0$, given any $\mu(\cdot) : [t_0, \infty) \to \mathbb{R}^4 \times \mathbb{R}^2$, $\mu(t_0) = \mu_0$, with $\|\mu_0\| \le r$, there is a finite time $T(\bar{d}, r) \ge 0$ such that $\|\mu(t)\| \le \bar{d}$ for all $t > t_0 + T(\bar{d}, r)$.

Theorem 1. *Suppose the uncertain system Equation (18) is subject to control Equation (19), with adaptive parameter $\hat{\beta}$ given by Equation (23). Let $\mu = [x^{\mathrm{T}}\ \hat{\beta}^{\mathrm{T}} - \beta^{\mathrm{T}}]^{\mathrm{T}}$, $\mu_0 = [x_0^{\mathrm{T}}\ \hat{\beta}_0^{\mathrm{T}} - \beta^{\mathrm{T}}]$. Then there exists a constant $d > 0$ such that the closed-loop system possesses the UB and UUB properties.*

Remark 1. Lemma 1 states that the matched uncertainty of the path tracking system is cone-bounded, which provides the studied sufficient condition for Theorem 1. Theorem 1 illustrates that the closed-loop system possesses UB and UUB properties. Convergence to the equilibrium state strictly is not possible for the uncertain system due to the unpredictable uncertainty. In fact, UUB is the best performance that the uncertain system can achieve. For any initial state, the final state can always return to a given sphere near the equilibrium state. In the real-world path tracking system, these properties guarantees bounded tracking error.

4 | PERFORMANCE ANALYSIS

In this section, we analyze the performance of the controller designed in Section 3. The process is divided into two parts, (1) verifying the deterministically guaranteed performance against matched uncertainties and (2) verifying the robustness against mismatched uncertainties.

4.1 | Proof of Theorem 1

Take the following Lyapunov function candidate

$$\begin{aligned} \tilde{v}(x, \hat{\beta}) &= \eta_1 v_1(x) + \eta_2 v_2(\hat{\beta}), \\ v_1(x) = x^{\mathrm{T}}Px,\ v_2(\hat{\beta}) &= \frac{1}{2}(\hat{\beta} - \beta)^{\mathrm{T}} L_1^{-1}(\hat{\beta} - \beta), \end{aligned} \tag{32}$$

where P is the solution of the Riccati equation (20), and positive constant coefficients η_1 and η_2 are to be decided later.

Taking the time derivative of v_1, it can be shown that

$$\begin{aligned} \dot{v}_1(x) &= 2x^{\mathrm{T}}P\dot{x} = 2x^{\mathrm{T}}P[\bar{A}x + Bp(x + w, \hat{\beta}) + B\hat{e} + BKw] \\ &= 2x^{\mathrm{T}}P[\bar{A}x + Bp(y, \beta) + B\hat{e} + BKw] + 2y^{\mathrm{T}}PB[p(y, \hat{\beta}) - p(y, \beta)] - 2w^{\mathrm{T}}PB[p(y, \hat{\beta}) - p(y, \beta)], \end{aligned} \tag{33}$$

where $\bar{A} \triangleq A + BK$, with K designed in Equation (21). For the first term of Equation (33) we have

$$2x^{\mathrm{T}}P[\bar{A}x + Bp(y, \beta) + B\hat{e} + BKw] \le -\lambda_m(Q)\|x\|^2 + \lambda_1\|x\| + \lambda_2, \tag{34}$$

where

$$\lambda_1 = \frac{\epsilon}{2}k_2, \quad \hat{w} = \max_{w \in W}\|w\|, \quad \lambda_2 = \frac{\epsilon}{2}[(2k_2 + \|K\|)\hat{w} + k_1], \tag{35}$$

is related to the bounds of uncertainties.[32]

As for the second term of the Equation (33), if $\|B^{\mathrm{T}}Py\| > \epsilon$,

$$\begin{aligned} 2y^{\mathrm{T}}PB[p(y,\hat{\beta}) - p(y,\beta)] &\leq -2\|B^{\mathrm{T}}Py\|^2\|B^{\mathrm{T}}Py\|^{-1} \times [(\hat{\beta}_1 - \beta_1) + (\hat{\beta}_2 - \beta_2)\|y\|] \\ &= -2\|B^{\mathrm{T}}Py\|g^{\mathrm{T}}(\hat{\beta} - \beta). \end{aligned} \tag{36}$$

Otherwise, for $\|B^{\mathrm{T}}Py\| \leq \epsilon$, we have

$$\begin{aligned} 2y^{\mathrm{T}}PB[p(y,\hat{\beta}) - p(y,\beta)] &\leq -2\|B^{\mathrm{T}}Py\|^2\epsilon^{-1}[(\hat{\beta}_1 - \beta_1) + (\hat{\beta}_2 - \beta_2)\|y\|] \\ &= -2\|B^{\mathrm{T}}Py\|^2\epsilon^{-1}g^{\mathrm{T}}(\hat{\beta} - \beta). \end{aligned} \tag{37}$$

Similarly, for $\|B^{\mathrm{T}}Py\| > \epsilon$, the third term of Equation (33) satisfies

$$\begin{aligned} -2w^{\mathrm{T}}PB[p(y,\hat{\beta}) - p(y,\beta)] &\leq 2(B^{\mathrm{T}}Pw)^{\mathrm{T}}(B^{\mathrm{T}}Py)\|B^{\mathrm{T}}Py\|^{-1}g^{\mathrm{T}}(\hat{\beta} - \beta) \\ &\leq 2\overline{w}\|B^{\mathrm{T}}Py\|\|B^{\mathrm{T}}Py\|^{-1}\|g\|\|\hat{\beta} - \beta\| \\ &= 2\overline{w}\|g\|\|\hat{\beta} - \beta\|, \end{aligned} \tag{38}$$

where $\overline{w} = \max_{w\in W}\|B^{\mathrm{T}}Pw\|$. Since

$$\|g\|^2 = 1 + \|y\|^2 \leq (1 + \|y\|)^2, \tag{39}$$

we have

$$2\overline{w}\|g\|\|\hat{\beta} - \beta\| \leq 2\overline{w}(1 + \|y\|)\|\hat{\beta} - \beta\|. \tag{40}$$

For $\|B^{\mathrm{T}}Py\| \leq \epsilon$,

$$\begin{aligned} -2w^{\mathrm{T}}PB[p(y,\hat{\beta}) - p(y,\beta)] &\leq 2\overline{w}\|B^{\mathrm{T}}Py\|\epsilon^{-1}(1 + \|y\|)\|\hat{\beta} - \beta\| \\ &\leq 2\overline{w}(1 + \|y\|)\|\hat{\beta} - \beta\|. \end{aligned} \tag{41}$$

The time derivative of v_2 is given as follows. For $\|B^{\mathrm{T}}Py\| > \epsilon$,

$$\begin{aligned} \dot{v}_2(\hat{\beta}) &= (\hat{\beta} - \beta)^{\mathrm{T}}L_1^{-1}(L_1 g\|B^{\mathrm{T}}Py\| - L_2\hat{\beta} - L_3\hat{\beta}\|y\|) \\ &= (\hat{\beta} - \beta)^{\mathrm{T}}g\|B^{\mathrm{T}}Py\| - (\hat{\beta} - \beta)^{\mathrm{T}}L_1^{-1}L_2(\hat{\beta} - \beta) - (\hat{\beta} - \beta)L_1^{-1}L_2\beta \\ &\quad - (\hat{\beta} - \beta)^{T}L_1^{-1}L_3(\hat{\beta} - \beta)\|y\| - (\hat{\beta} - \beta)^{\mathrm{T}}L_1^{-1}L_3\beta\|y\|. \end{aligned} \tag{42}$$

Combining Equations (32), (34), (36), and (38), we can obtain the total time derivative of Lyapunov function for $\|B^{\mathrm{T}}Py\| > \epsilon$,

$$\begin{aligned} \dot{\hat{v}}(x,\hat{\beta}) &\leq -\eta_1\lambda_m(Q)\|x\|^2 + \eta_1\lambda_1\|x\| + \eta_1\lambda_2 - 2\eta_1\|B^{\mathrm{T}}Py\|g^{\mathrm{T}}\|\hat{\beta} - \beta\| + 2\eta_1\overline{w}\|y\|\|\hat{\beta} - \beta\| \\ &\quad + 2\eta_1\overline{w}\|\hat{\beta} - \beta\| + \eta_2(\hat{\beta} - \beta)^{\mathrm{T}}g\|B^{\mathrm{T}}Py\| - \eta_2(\hat{\beta} - \beta)^{\mathrm{T}}L_1^{-1}L_2\beta \\ &\quad - \eta_2(\hat{\beta} - \beta)^{T}L_1^{-1}L_3(\hat{\beta} - \beta)\|y\| - \eta_2(\hat{\beta} - \beta)^{\mathrm{T}}L_1^{-1}L_3\beta\|y\|. \end{aligned} \tag{43}$$

Here choose $2\eta_1 = \eta_2$ and let $\overline{\beta} \triangleq \|\beta\|$, and observe the fact that

$$\begin{aligned} &2\eta_1\overline{w}\|y\|\|\hat{\beta} - \beta\| - \eta_2(\hat{\beta} - \beta)^{\mathrm{T}}L_1^{-1}L_2(\hat{\beta} - \beta)\|y\| - \eta_2(\hat{\beta} - \beta)^{\mathrm{T}}L_1^{-1}L_3\beta\|y\| \\ &\leq [(2\eta_1\overline{w} + \eta_2\overline{\beta}\lambda_M(L_1^{-1}L_3))\|\hat{\beta} - \beta\| - \eta_2\lambda_m(L_1^{-1}L_2)\|\hat{\beta} - \beta\|^2]\|y\| \\ &\leq [4\eta_2\lambda_m(L_1^{-1}L_2)]^{-1} \times [2\eta_1\overline{w} + \eta_2\overline{\beta}\lambda_M(L_1^{-1}L_3)]^2\|y\| \\ &\triangleq \lambda_3\|y\| \leq \lambda_3\|x\| + \lambda_3\hat{w}. \end{aligned} \tag{44}$$

Then, for $\|B^{\mathrm{T}}Py\| > \epsilon$, it turns out that

$$\dot{\tilde{v}} \leq -\eta_1\lambda_m(Q)\|x\|^2 + (\eta_1\lambda_1 + \lambda_3)\|x\| + \eta_1\lambda_2 + \lambda_3\hat{w} - \eta_2\lambda_m(L_1^{-1}L_2)\|\hat{\beta} - \beta\|^2 + [2\eta_1\overline{w} + \eta_2\overline{\beta}\lambda_M(L_1^{-1}L_2)]\|\hat{\beta} - \beta\|. \tag{45}$$

Following the similar procedure, combine Equations (32), (34), (37), and (41) we can obtain the same results, for $\|B^{\mathrm{T}}Py\| \leq \epsilon$ unequal relationship (45) holds too.

Now let $\mu = [x^{\mathrm{T}}\ \hat{\beta}^{\mathrm{T}} - \beta^{\mathrm{T}}]^{\mathrm{T}}$ and hence $\|\mu\|^2 = \|x\|^2 + \|\hat{\beta} - \beta\|^2$, it turns out that for both $\|B^{\mathrm{T}}Py\| > \epsilon$ and $\|B^{\mathrm{T}}Py\| \leq \epsilon$,

$$\dot{\tilde{v}} \leq -\lambda_4\|\mu\|^2 + \lambda_5\|\mu\| + \lambda_6, \tag{46}$$

where

$$\begin{aligned}
\lambda_4 &= \min\{\eta_1\lambda_m(Q), \eta_2\lambda_m(L_1^{-1}L_2)\},\\
\lambda_5 &= [(\eta_1\lambda_1 + \lambda_3)^2 + (2\eta_1\overline{w} + \eta_2\overline{\beta}\lambda_M(L_1^{-1}L_2))^2]^{\frac{1}{2}},\\
\lambda_6 &= \eta_1\lambda_2 + \lambda_3\overline{w}.
\end{aligned} \tag{47}$$

By choosing appropriate matrices Q, L_1, and L_2, we can assure $\lambda_4 > 0$. In this case, $\dot{\tilde{v}}$ is negative definite for any sufficiently large $\|\mu\|$, which satisfies

$$\|\mu\| > \frac{\lambda_5 + \sqrt{\lambda_5^2 + 4\lambda_4\lambda_6}}{2\lambda_4}. \tag{48}$$

We conclude the uniform boundedness with

$$d(r) = \begin{cases} \sqrt{\frac{\gamma_2}{\gamma_1}}\tilde{R} & \text{if } r \leq \tilde{R} \\ \sqrt{\frac{\gamma_2}{\gamma_1}}r & \text{otherwise,} \end{cases} \tag{49}$$

where

$$\begin{aligned}
\gamma_1 = \min\{\eta_1\lambda_m(P), \eta_2\lambda_m(L_1^{-1})/2\}, \quad \gamma_2 = \max\{\eta_1\lambda_M(P), \eta_2\lambda_M(L_1^{-1})/2\},\\
\tilde{R} = \frac{\lambda_5 + \sqrt{\lambda_5^2 + 4\lambda_4\lambda_6}}{2\lambda_4}.
\end{aligned} \tag{50}$$

Furthermore, the system possesses uniformly ultimate boundedness characteristic, because with $\|x_0\| < r$, there exists

$$T(\overline{d}, r) = \begin{cases} 0 & \text{if } r \leq \overline{R} \\ \frac{\gamma_2 r^2 - \gamma_1^2\gamma_2^{-1}\overline{d}^2}{\lambda_4\gamma_1\gamma_2^{-1}\overline{d}^2 - \lambda_5\sqrt{\gamma_1/\gamma_2}\overline{d} - \lambda_6} & \text{otherwise,} \end{cases} \tag{51}$$

where $\overline{R} = \sqrt{\frac{\gamma_1}{\gamma_2}}\overline{d}$.

Remark 2. This subsection presents the proof of the UB and UUB properties of the closed-loop system. The proof is supported by Lyapunov stability theory. We take a positive definite Lyapunov function candidate regarding state x and adaptive parameter $\hat{\beta}$, and then verify the negative definiteness of its time derivative using some inequality scaling tricks. Equations (49) and (51) indicate the uniform boundedness and ultimate boundedness region.

4.2 | Robustness against mismatched uncertainties

The previous subsection designs an adaptive robust control (ARC) and analyzes its performance, which considers only matched uncertainties in the path tracking system. It is of practical significance that the proposed control be robust against

the presence of mismatched uncertainties.[33] Therefore, this subsection studies the robustness of the proposed controller against mismatched uncertainties.

In Equation (16), we have decomposed the uncertainties into matched portion $e(x,t)$ and mismatched portion $\tilde{e}(x,t)$, as shown in Equation (17). Suppose that there are constants $\delta_1, \delta_2 \geq 0$ such that for all $(x,t) \in \mathbb{R}^4 \times \mathbb{R}$, the mismatched portion is also cone-bounded, that is,

$$\|\tilde{e}(x,t)\| \leq \delta_1 + \delta_2 \|x\|. \tag{52}$$

Assumption Equation (52) is valid in path tracking system, because according to Equation (17), we have

$$\|\tilde{e}\| = \|A_2 x + D_1 c_R\| \leq \|A_2\|\|x\| + \|D_1 c_R\|. \tag{53}$$

Then, consider the Lyapunov function candidate $\tilde{v}$ same as Equation (32), if the mismatched uncertainty $\tilde{e}$ is added, the time derivative of v_1 can be written as

$$\dot{v}_1(x) = 2x^{\mathrm{T}} P[\bar{A}x + Bp(y,\beta) + B\hat{e} + BKw] + 2y^{\mathrm{T}} PB[p(y,\hat{\beta}) - p(y,\beta)] - 2w^{\mathrm{T}} PB[p(y,\hat{\beta}) - p(y,\beta)] + 2x^{\mathrm{T}} P\tilde{e}. \tag{54}$$

Compared with the original equation, an extra term $2x^{\mathrm{T}} P\tilde{e}$ is introduced. Combine Equation (54), the term can be scaled as follows

$$\begin{aligned} 2x^{\mathrm{T}} P\tilde{e} &\leq 2\|x^{\mathrm{T}} P\|\|\tilde{e}\| \\ &\leq 2\|x^{\mathrm{T}} P\|(\delta_1 + \delta_2\|x\|) \\ &\leq 2\delta_1\|x\|\|P\| + 2\delta_2\|x\|^2\|P\| \\ &\leq 2\delta_1\lambda_M(P)\|x\| + 2\delta_2\lambda_M(P)\|x\|^2. \end{aligned} \tag{55}$$

Upon performing the similar procedure as Equations (33)–(47), with the incorporation of Equation (55), the time derivative of Lyapunov function candidate is then given by

$$\dot{\tilde{v}} \leq -\tilde{\lambda}_4\|\mu\|^2 + \tilde{\lambda}_5\|\mu\| + \tilde{\lambda}_6, \tag{56}$$

where

$$\begin{aligned} \tilde{\lambda}_4 &= \min\{\eta_1\lambda_m(Q) - 2\eta_1\delta_2\lambda_M(P), \eta_2\lambda_m(L_1^{-1}L_2)\}, \\ \tilde{\lambda}_5 &= [(\eta_1\lambda_1 + \lambda_3 + 2\eta_1\delta_1\lambda_M(P))^2 + (2\eta_1\overline{w} + \eta_2\overline{\beta}\lambda_M(L_1^{-1}L_2))^2]^{\frac{1}{2}}, \\ \tilde{\lambda}_6 &= \lambda_6 = \eta_1\lambda_2 + \lambda_3\overline{w}. \end{aligned} \tag{57}$$

Provided the constant δ_2 satisfies

$$\delta_2 < \frac{\lambda_m(Q)}{2\lambda_M(P)}, \tag{58}$$

$\tilde{\lambda}_4$ is guaranteed to be positive. By replacing λ_4 and λ_5 by $\tilde{\lambda}_4$ and $\tilde{\lambda}_5$, and following the procedure similar to Equations (49)–(51), we can prove that the UB and UUB properties are still valid. That is, as long as the condition Equation (58) is given, the closed-loop system also shows robustness to mismatched uncertainties. The value δ_1 can still be arbitrarily large at the cost of increasing the size of the ultimate boundedness. The inequality (58) imposes an upper bound on δ_2, which depends on the ratio $\lambda_m(Q)/2\lambda_M(P)$. This ratio is only dependent on the nominal portion of the uncertain system. In the process of controller design that stabilizes the nominal system, we can select weighting matrices based on estimated δ_2, and make sure that the condition (58) holds.

5 | SIMULATION AND EXPERIMENTAL RESULTS

To validate the effectiveness of the controller, we conduct both simulation and field tests. This section describes the details of the simulation and vehicle experiments and discusses the results.

5.1 | Simulation results

We utilize TruckSim and MATLAB/Simulink co-simulation to evaluate the controller before real vehicle implementation. The vehicle dynamics are simulated by TruckSim and the controller is implemented in MATLAB/Simulink. The longitudinal motion is controlled by the PID controller in TruckSim to maintain a constant speed, and the lateral motion control input is provided by the proposed controller. A 2-axles tractor, which keeps pace with the vehicle platform in the field test, is chosen in the simulation. The parameters for the nominal part of the vehicle platform are listed in Table 2. The paths to be tracked include double lane change (DLC) and serpentine driving (SD) trajectory. The coordinates of the path points are the same as the setup in the literature.[34] To simulate the measurement noises, we add Gaussian noise with variance $\sigma = 0.02$ to the measured absolute location coordinates. The time step of the vehicle dynamic model update is chosen as 0.001 s, while the control time step is 0.02 s, which is close to the experimental vehicle system.

In both scenarios, the performance of the LQR and ARC controller is compared. Our designed adaptive robust control law is based on LQR control. It aims to compensate for the uncertainties and measurement noises. Hence, to validate the effectiveness of ARC, we select the same weighting matrices as that of LQR. The weighting matrices Q and R are given as

$$Q = \begin{bmatrix} 1 & 0 & 0 & 0 \\ 0 & 0.1 & 0 & 0 \\ 0 & 0 & 0.1 & 0 \\ 0 & 0 & 0 & 0.1 \end{bmatrix}, \quad R = 10. \tag{59}$$

The positive definite matrices in the proposed adaptive scheme for $\hat{\beta}$ are selected as

$$L_1 = \begin{bmatrix} 0.05 & 0 \\ 0 & 0.05 \end{bmatrix}, L_2 = \begin{bmatrix} 1 & 0 \\ 0 & 1 \end{bmatrix}, L_3 = \begin{bmatrix} 1 & 0 \\ 0 & 1 \end{bmatrix} \tag{60}$$

Figures 2 and 3 show the simulation results of the proposed ARC and the comparison with the baseline LQR controller. Table 3 lists the evaluation metrics of LQR and ARC.

5.1.1 | Case 1: DLC scenario

First, the simulation is carried out in the double lane change scenario. The target longitudinal speed is set as 60 km/h. The speed control is fulfilled by TruckSim, which confirms vehicle dynamics. Figure 2 depicts the simulation results of path tracking performance and control input. Figure 2A displays the global path of the vehicle controlled by LQR or ARC, which shows that ARC achieves better tracking performance than LQR control does, especially when the vehicle is steering. This is because the additional control force in ARC counteracts the impact of the uncertainties from vehicle dynamics. Figure 2B,C illustrate the lateral error and heading error during the simulation. The peak values of both errors decrease. We use the root mean square (RMS) value of the error to evaluate the performance of the controller. As is listed in Table 3, the RMS of lateral error under ARC is 0.0102, which is about 31.8% lower than it of LQR control. The control

TABLE 2 Simulation parameters setup

Symbol	m	l_f	l_r	$\overline{C}_f$	$\overline{C}_r$	I_z
Value	5760 (kg)	1.11 (m)	3.89 (m)	1.4×10^5 (N/rad)	2.2×10^5 (N/rad)	34,802 (kg m^2)

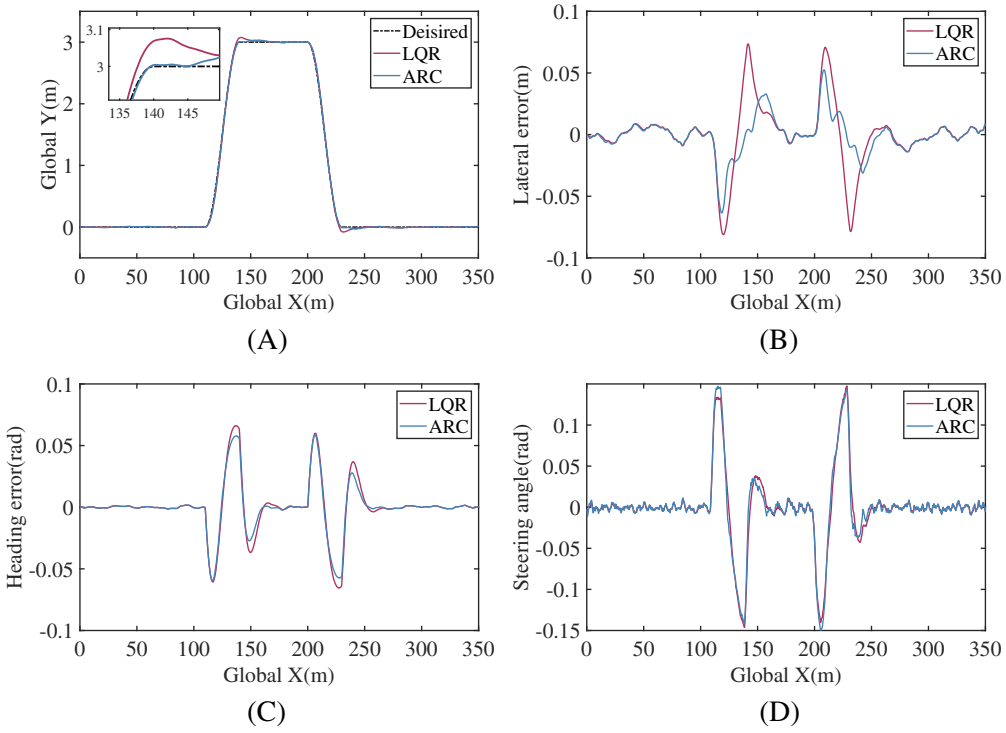

FIGURE 2 Comparison of tracking performance under 60 km/h DLC scenario. (A) Global path. (B) Lateral error. (C) Heading error. (D) Front-wheel steering angle

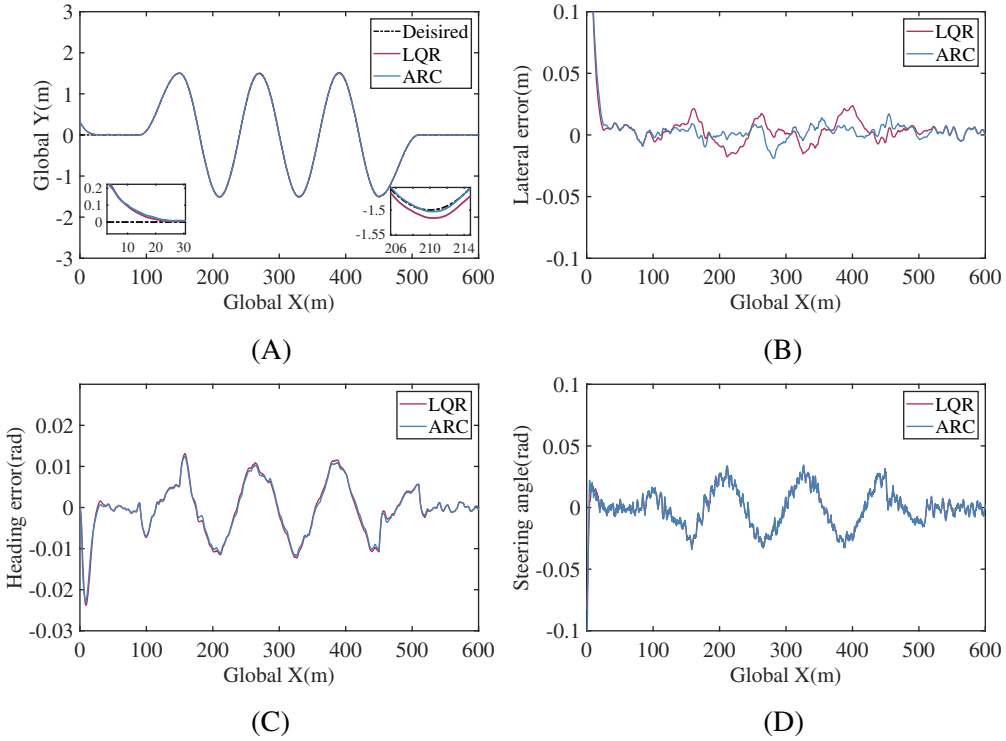

FIGURE 3 Comparison of tracking performance under 60 km/h SD scenario. (A) Global path. (B) Lateral error. (C) Heading error. (D) Front-wheel steering angle

TABLE 3 Comparison of the quantitative results

	DLC simulation		SD simulation		Field test	
	LQR	ARC	LQR	ARC	LQR	ARC
RMS of lateral error	0.0149	0.0102	0.0089	0.0059	0.2365	0.1690
RMS of heading error	0.0120	0.0107	0.0062	0.0060	0.0549	0.0354
RMS of control input[a]	0.0238	0.0241	0.0182	0.0192	2.6675	2.6473

[a]Front wheel steering angle in simulations and steering wheel angle in the field test.

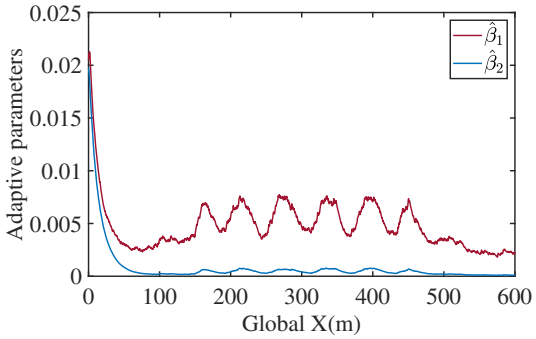

FIGURE 4 Adaptive parameters in SD scenario

input, that is, the front wheel steering angle, is shown in Figure 2D. We find that ARC's RMS value of steering angle, which indicates the control effort, is larger than that of LQR control. It means that the robustness against the uncertainties is at the cost of extra control effort.

5.1.2 | Case 2: Serpentine driving scenario

We then test the ARC controller in the serpentine driving scenario. The longitudinal speed of the vehicle is maintained at 60 km/h. To display the transient performance of the designed ARC controller, we add a 0.3 m lateral offset in the initial state. As can be seen in Figure 3A, the adaptive robust control renders the desired system performance. Figure 3B demonstrates that when the vehicle is steering, the ARC has a more stable performance than the LQR controller. In this scenario, the quantitative results are calculated by the data that satisfies the X coordinate in [50,600]m, which is not influenced by the initial error. As is listed in Table 3, the RMS of lateral error under ARC is 0.0059, which is about 33.7% lower than that of LQR control. In this scenario, the RMS of the steering angle is slightly smaller than that of LQR. This demonstrates that the introduction of the robust control term does not always cost extra effort. Besides, Figure 4 shows the curves of adaptive parameters $\hat{\beta}_1$ and $\hat{\beta}_2$. The curves demonstrate that the designed adaptive scheme can follow the change of the uncertainties and approximate its bound.

5.2 | Experimental results

To validate the effectiveness of the designed controller against uncertainties in real-world engineering systems, we implement it on a vehicle platform. The platform is Jiefang J6P, a 2-axles tractor, as shown in Figure 5. It is equipped with a by-wire control system that allows for automation of steering, throttle, and brake. The Npos320 integrated navigation system (INS) is utilized to acquire kinematic information, including vehicle real-time position, longitudinal speed, lateral speed, and yaw angle. The localization accuracy of the INS is 0.04 m. The actual steering angle of the steering wheel is measured through the Bosch angle sensor. All of this information is sent to the NVIDIA TX2 computing platform by serial port or CAN bus. The designed controller is implemented in C++ under the Cyber RT framework. The speed of the vehicle is also maintained by a PID controller. The experiments are conducted in a flat and open field. Before testing the

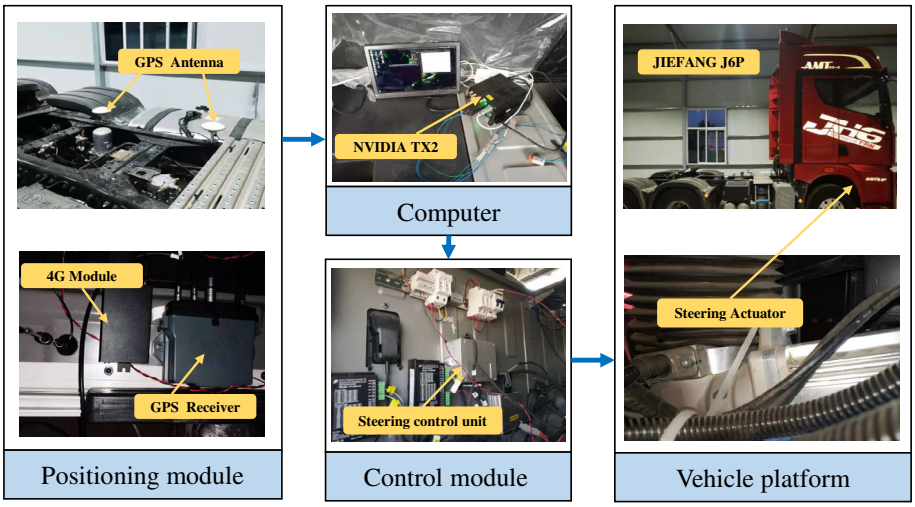

FIGURE 5 Structure of the vehicle platform

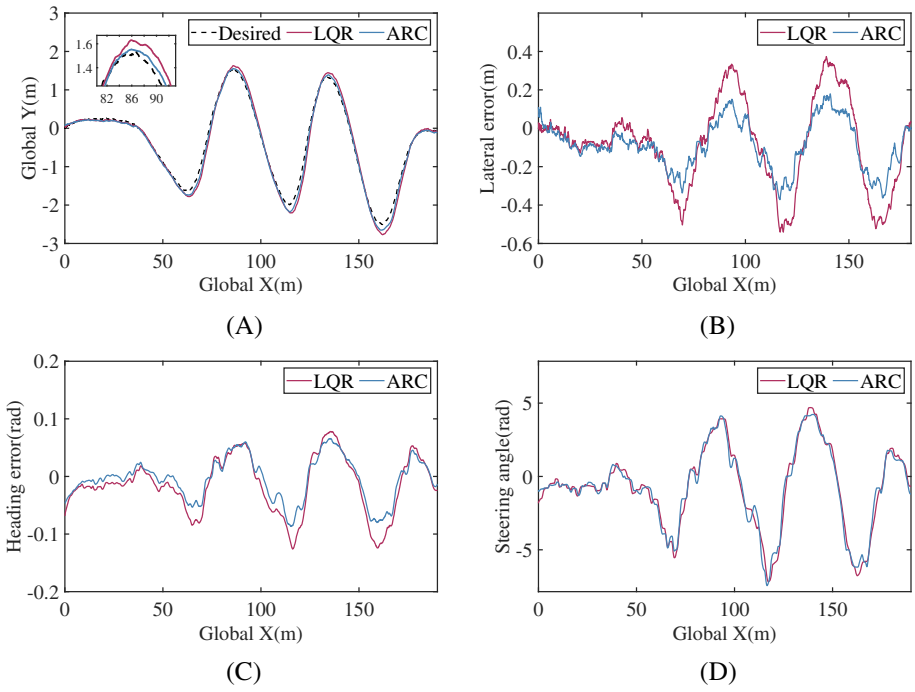

FIGURE 6 Comparison of tracking performance in the field test. (A) Global path. (B) Lateral error. (C) Heading error. (D) Steering wheel angle

control algorithm, the vehicle is driven manually to record a serpentine path as the desired path. At the beginning of each trial, the vehicle starts at the same location and tracks the desired path autonomously using the developed path tracking control algorithm. The experimental validation results are shown in Figure 6.

The experiment is carried out in the serpentine driving scenario. The target longitudinal speed is set as 30 km/h, which is fulfilled using the by-wire throttle and brake system. Figure 6A depicts the tracking performance of the two control strategies. Similar to simulation results, the curvature near the trajectory is large, and the tracking performance is poor. Figure 6B,C illustrate the lateral error and the heading error. Table 3 lists the tracking performance of the two controllers in the field experiment. The proposed ARC has a great improvement on both lateral error and heading error. The enhanced tracking accuracy is larger than the localization accuracy of INS, which indicates that the improvement results from the control algorithm instead of the localization error. Compared with the simulation results, the improvement is more dominant, because in the real-world vehicle system the uncertainties are more complex, and may have a great impact

on the controllers without considering them. The RMS of the steering wheel angle in the experiment is 2.6473, slightly smaller than the LQR controller, which indicates that the improvement of performance does not always come with extra control efforts.

6 | CONCLUSION

In this article, an adaptive robust path tracking control strategy for autonomous vehicles is developed and investigated. First, the path tracking dynamic model is formulated, based on a single-track bicycle model and considering parametric uncertainties. Second, the proposed control law is based on the linear quadratic regulator control framework, which is used to stabilize the nominal part of the system. The robust control law with an adaptive scheme is designed to counteract the impact of model uncertainties and measurement noises. Third, we analyze the performance of the closed-loop system and demonstrate that it possesses uniform boundedness and uniform ultimate boundedness properties. The robustness against the mismatched uncertainties of the control law is also proved.

The designed path tracking controller is implemented both on the simulation platform, by using MATLAB/Simulink and TruckSim, and on a real autonomous vehicle. The experimental results support the effectiveness of the proposed strategy. The conclusions are drawn as follows: (a) The proposed control strategy can deal with system uncertainties and measurement noises at the same time, with a great improvement in tracking accuracy. (b) The adaptive scheme has the capability to approximate the bounds of the uncertainties.

In this article, we focus on the parametric uncertainties in the system modeling. In fact, uncertainties in the path tracking task may come from many other sources, such as external disturbance and time delay. Further investigations on the robustness against these uncertain systems are worth pursuing in the future work.

ACKNOWLEDGMENT

This research is sponsored in part by the National Natural Science Foundation of China (NSFC) (No. 61872217, No. U20A20285, No. 52122217, No. U1801263), the research is also sponsored in part by the Ministry of Science and Technology of the People's Republic of China (No. 2020YFB1710901).

CONFLICT OF INTEREST

The authors declare no potential conflict of interests.

DATA AVAILABILITY STATEMENT

The data supporting the findings of this study are available from the corresponding author upon reasonable request.

ORCID

Huiqian Li https://orcid.org/0000-0003-4949-8834
Zeyu Yang https://orcid.org/0000-0002-7232-5678

REFERENCES

1. Yao Q, Tian Y, Wang Q, Wang S. Control strategies on path tracking for autonomous vehicle: state of the art and future challenges. *IEEE Access*. 2020;8:161211-161222. doi:10.1109/ACCESS.2020.3020075
2. Zhang X, Zhu X. Autonomous path tracking control of intelligent electric vehicles based on lane detection and optimal preview method. *Expert Syst Appl*. 2019;121:38-48. doi:10.1016/j.eswa.2018.12.005
3. Sun Z, Wang R, Ye Q, Wei Z, Yan B. Investigation of intelligent vehicle path tracking based on longitudinal and lateral coordinated control. *IEEE Access*. 2020;8:105031-105046. doi:10.1109/ACCESS.2020.2994437
4. Hu C, Wang Z, Taghavifar H, et al. MME-EKF-based path-tracking control of autonomous vehicles considering input saturation. *IEEE Trans Veh Technol*. 2019;68(6):5246-5259. doi:10.1109/TVT.2019.2907696
5. Xu S, Peng H. Design, analysis, and experiments of preview path tracking control for autonomous vehicles. *IEEE Trans Intell Transp Syst*. 2020;21(1):48-58. doi:10.1109/TITS.2019.2892926
6. Xu S, Peng H, Tang Y, Member S. Preview path tracking control with delay compensation for autonomous vehicles. *IEEE Trans Intell Transp Syst*. 2020;22(5):2979-2989.
7. Zhang X, Wang Y, Yang Z, Huang J, Su Y. Path tracking control for autonomous vehicles with saturated input: a fuzzy fixed-time learning control approach. *IET Intell Transp Syst*. 2021;2022:1-12. doi:10.1049/itr2.12156
8. Shan Y, Zheng B, Chen L, Chen L, Chen D. A reinforcement learning-based adaptive path tracking approach for autonomous driving. *IEEE Trans Veh Technol*. 2020;69(10):10581-10595. doi:10.1109/TVT.2020.3014628

9. Lu Y, Li W, Zhang X, Xu X. Continuous-time receding-horizon reinforcement learning and its application to path-tracking control of autonomous ground vehicles. *Opt Control Appl Methods*. 2021;April:1-19. doi:10.1002/oca.2832
10. Amer NH, Zamzuri H, Hudha K, Kadir ZA. Modelling and control strategies in path tracking control for autonomous ground vehicles: a review of state of the art and challenges. *J Intell Robot Syst Theory Appl*. 2017;86(2):225-254. doi:10.1007/s10846-016-0442-0
11. Coulter RC. Implementation of the pure pursuit path tracking algorithm. Carnegie-Mellon UNIV Pittsburgh PA Robotics INST; 1992.
12. Hoffmann GM, Tomlin CJ, Montemerlo M, Thrun S. Autonomous automobile trajectory tracking for off-road driving: controller design, experimental validation and racing. Proceedings of the American Control Conference 2007:2296-2301. doi: 10.1109/ACC.2007.4282788
13. Cordeiro RA, Azinheira JR, De Paiva EC, Bueno SS. Dynamic modeling and bio-inspired LQR approach for off-road robotic vehicle path tracking. Proceedings of the 2013 16th International Conference on Advanced Robotics, ICAR 2013; 2013. doi: 10.1109/ICAR.2013.6766549
14. Guo H, Cao D, Chen H, Sun Z, Hu Y. Model predictive path following control for autonomous cars considering a measurable disturbance: implementation, testing, and verification. *Mech Syst Signal Process*. 2019;118:41-60. doi:10.1016/j.ymssp.2018.08.028
15. Zhang C, Hu J, Qiu J, Yang W, Sun H, Chen Q. A novel fuzzy observer-based steering control approach for path tracking in autonomous vehicles. *IEEE Trans Fuzzy Syst*. 2019;27(2):278-290. doi:10.1109/TFUZZ.2018.2856187
16. Jha B, Turetsky V, Shima T. Robust path tracking by a dubins ground vehicle. *IEEE Trans Control Syst Technol*. 2019;27(6):2614-2621. doi:10.1109/TCST.2018.2870571
17. Mata S, Zubizarreta A, Pinto C. Robust tube-based model predictive control for lateral path tracking. *IEEE Trans Intell Veh*. 2019;4(4):569-577. doi:10.1109/TIV.2019.2938102
18. Yang Z, Huang J, Hu Z, Yin H, Zhong Z. Adaptive constraint-following control for uncertain nonlinear mechanical systems with measurement error. *Int J Robust Nonlinear Control*. 2021;31(10):4823-4838. doi:10.1002/rnc.5506
19. Chen C, Shu M, Wang Y, Liu R. Robust control for path tracking of network-based autonomous vehicles. *Math Probl Eng*. 2020;2020:2537086. doi:10.1155/2020/2537086
20. Tagne G, Talj R, Charara A. Design and comparison of robust nonlinear controllers for the lateral dynamics of intelligent vehicles. *IEEE Trans Intell Transp Syst*. 2016;17(3):796-809. doi:10.1109/TITS.2015.2486815
21. Peng H, Wang W, An Q, Xiang C, Li L. Path tracking and direct yaw moment coordinated control based on robust MPC with the finite time horizon for autonomous independent-drive vehicles. *IEEE Trans Veh Technol*. 2020;69(6):6053-6066. doi:10.1109/TVT.2020.2981619
22. Sun T, Pan Y, Zhang J, Yu H. Robust model predictive control for constrained continuous-time nonlinear systems. *Int J Control*. 2018;91(2):359-368. doi:10.1080/00207179.2017.1282177
23. Lee K, Jeon S, Kim H, Kum D. Optimal path tracking control of autonomous vehicle: adaptive full-state linear quadratic Gaussian (LQG) control. *IEEE Access*. 2019;7:109120-109133. doi:10.1109/access.2019.2933895
24. Gao Z, Guo G. Command filtered path tracking control of saturated ASVs based on time-varying disturbance observer. *Asian J Control*. 2020;22(3):1197-1210. doi:10.1002/asjc.1990
25. Chen S, Song K, Zhao L, Xue W, Xie H, Huang Y. On active disturbance rejection based path following control for unmanned roller. Proceedings of the IEEE Conference on Decision and Control 2019; 2019-Decem(Cdc); 2019:4791-4796; IEEE. doi: 10.1109/CDC40024.2019.9029669
26. Mohan Rayguru M, Rajesh Elara M, Ramalingam B, Muthugala MAV, Samarakoon SMP. A path tracking strategy for car like robots with sensor unpredictability and measurement errors. *Sensors (Switzerland)*. 2020;20(11):3077. doi:10.3390/s20113077
27. Zuo Z, Liu C, Han QL, Song J. Unmanned aerial vehicles: control methods and future challenges. *IEEE/CAA J Automat Sin*. 2022;99:1-14. doi:10.1109/JAS.2022.105410
28. Brudigam T, Olbrich M, Leibold M, Wollherr D. Combining stochastic and scenario model predictive control to handle target vehicle uncertainty in an autonomous driving highway scenario. Proceedings of the IEEE Conference on Intelligent Transportation Systems, Proceedings, ITSC 2018; November 2018:1317-1324. doi: 10.1109/ITSC.2018.8569909
29. Yoo C, Anstee S, Fitch R. Stochastic path planning for autonomous underwater gliders with safety constraints. Proceedings of the IEEE International Conference on Intelligent Robots and Systems; 2019:3725-3732. doi: 10.1109/IROS40897.2019.8968250
30. Xu J, Du Y, Chen YH, Guo H. Optimal robust control design for constrained uncertain systems: a fuzzy-set theoretic approach. *IEEE Trans Fuzzy Syst*. 2018;26(6):3494-3505. doi:10.1109/TFUZZ.2018.2834320
31. Zhang L, Ding H, Shi J, et al. An adaptive backstepping sliding mode controller to improve vehicle maneuverability and stability via torque vectoring control. *IEEE Trans Veh Technol*. 2020;69(3):2598-2612. doi:10.1109/TVT.2019.2950219
32. Leitmann G. On the efficacy of nonlinear control in uncertain linear systems. *J Dyn Syst Measur Control Trans ASME*. 1981;103(2):95-102. doi:10.1115/1.3139661
33. Chen YH. Adaptive robust control of uncertain systems with measurement noise. *Automatica*. 1992;28(4):715-728. doi:10.1016/0005-1098(92)90032-B
34. Ji X, Liu Y, He X, et al. Interactive control paradigm-based robust lateral stability controller design for autonomous automobile path tracking with uncertain disturbance: a dynamic game approach. *IEEE Trans Veh Technol*. 2018;67(8):6906-6920. doi:10.1109/TVT.2018.2834381

How to cite this article: Li H, Huang J, Yang Z, Hu Z, Yang D, Zhong Z. Adaptive robust path tracking control for autonomous vehicles with measurement noise. *Int J Robust Nonlinear Control*. 2022;1-17. doi: 10.1002/rnc.6218